APPLIED AND ENVIRONMENTAL MICROBIOLOGY, July 2005, p. 3725–3733 Vol. 71, No. 7
0099-2240/05/$08.00+0 doi:10.1128/AEM.71.7.3725–3733.2005

Growth and Population Dynamics of Anaerobic Methane-Oxidizing Archaea and Sulfate-Reducing Bacteria in a Continuous-Flow Bioreactor

Peter R. Girguis,[1] Aaron E. Cozen,[2] and Edward F. DeLong[3]*

Monterey Bay Aquarium Research Institute, 7700 Sandholdt Road, Moss Landing, California 95039[1]; University of California, Santa Cruz, 225 Sinsheimer, Santa Cruz, California 95064[2]; and Massachusetts Institute of Technology, Department of Civil & Environmental Engineering, 15 Vassar St., 48-427, Cambridge, Massachusetts 02139-4307[3]

Received 9 November 2004/Accepted 8 February 2005

The consumption of methane in anoxic marine sediments is a biogeochemical phenomenon mediated by two archaeal groups (ANME-1 and ANME-2) that exist syntrophically with sulfate-reducing bacteria. These anaerobic methanotrophs have yet to be recovered in pure culture, and key aspects of their ecology and physiology remain poorly understood. To characterize the growth and physiology of these anaerobic methanotrophs and the syntrophic sulfate-reducing bacteria, we incubated marine sediments using an anoxic, continuous-flow bioreactor during two experiments at different advective porewater flow rates. We examined the growth kinetics of anaerobic methanotrophs and *Desulfosarcina*-like sulfate-reducing bacteria using quantitative PCR as a proxy for cell counts, and measured methane oxidation rates using membrane-inlet mass spectrometry. Our data show that the specific growth rates of ANME-1 and ANME-2 archaea differed in response to porewater flow rates. ANME-2 methanotrophs had the highest rates in lower-flow regimes ($\mu_{\text{ANME-2}} = 0.167 \cdot \text{week}^{-1}$), whereas ANME-1 methanotrophs had the highest rates in higher-flow regimes ($\mu_{\text{ANME-1}} = 0.218 \cdot \text{week}^{-1}$). In both incubations, *Desulfosarcina*-like sulfate-reducing bacterial growth rates were approximately $0.3 \cdot \text{week}^{-1}$, and their growth dynamics suggested that sulfate-reducing bacterial growth might be facilitated by, but not dependent upon, an established anaerobic methanotrophic population. ANME-1 growth rates corroborate field observations that ANME-1 archaea flourish in higher-flow regimes. Our growth and methane oxidation rates jointly demonstrate that anaerobic methanotrophs are capable of attaining substantial growth over a range of environmental conditions used in these experiments, including relatively low methane partial pressures.

Geochemical studies have shown that the anaerobic oxidation of methane (AOM) in marine sediments is a microbially mediated phenomenon and represents a significant component of carbon cycling in marine environments (4, 25, 32). Based on field and laboratory experiments and observations using rRNA-targeted fluorescent in situ hybridization, AOM is believed to be mediated by a consortium of archaea and sulfate-reducing bacteria (2, 5, 7, 20). Phylogenetic and isotopic analyses have shown that two groups of anaerobic methanotrophic archaea (ANME-1 and ANME-2) cooccur in sediments with sulfate-reducing bacteria and incorporate methane-derived carbon into cellular biomass (19, 30). Genomic and biochemical analyses suggest that microbial AOM may be achieved in part by reversal of the canonical methanogenic pathway (15, 23), and ongoing studies have shown that ANME-1 and ANME-2 methane-oxidizing archaea (or MOA) are distributed throughout the world in anoxic marine sediments where methane and sulfate are available (22, 26, 31, 35, 37, 39, 41).

Our understanding of MOA physiology has been advanced by employing both in situ isotopic tracers and serum vial incubations to examine the relation between AOM and sulfate reduction and the effect of physical factors, such as pressure and temperature, on MOA methane oxidation rates (1, 8, 9, 16, 20, 27, 40). Whereas these studies have identified the primary metabolites used by the consortia and the influence of some environmental parameters on metabolite consumption, much remains to be learned about MOA, including some basic aspects of MOA ecology and physiology, such as population growth rates and modes of syntrophic metabolite exchange. In addition, how environmentally relevant physicochemical conditions affect MOA biological processes in situ, such as metabolic and population growth rates, also remains to be determined.

To date no MOA have been isolated in pure culture. However, MOA have been grown in mixed communities during anaerobic incubations on a novel continuous-flow bioreactor called AMIS (14). In the current study, we used the AMIS to examine the relation between MOA and *Desulfosarcina*-like sulfate-reducing bacteria (*D*SRB) growth and population dynamics, as well as the effect of porewater flow rates on both MOA and *D*SRB growth, by incubating sediments collected from within and outside a hydrocarbon cold seep on the AMIS at low and higher porewater flow rates, respectively. During the incubations, sediments were sampled periodically, and the small-subunit (SSU) rRNA genes of ANME-1 and ANME-2 archaea, as well as those of *Desulfosarcina*-like sulfate-reducing bacteria, were quantified via quantitative PCRs (qPCRs) as a proxy for cell densities. qPCR has proven to be a reliable proxy for cell numbers and can be used when direct cell counts

* Corresponding author. Mailing address: Massachusetts Institute of Technology, Department of Civil & Environmental Engineering, 15 Vassar St., 48-427, Cambridge, MA 02139-4307. Phone: (617) 253-5271. Fax: (617) 258-8850. E-mail: delong@mit.edu.

prove to be unreliable for quantification (14, 34). In addition, we measured sediment methane and sulfate concentrations, as well as methane oxidation rates prior to and after incubation. These data were used to determine the specific growth rates of different MOA and *D*SRB at low and higher porewater flow rates, to examine the population growth dynamics between ANME-1 MOA, ANME-2 MOA, and *D*SRB phylotypes, and to assess the effect of the porewater flow rate on MOA methane metabolism.

MATERIALS AND METHODS

Experimental overview. Sediments were collected from within and outside a hydrocarbon seep in the Monterey canyon and will hereafter be referred to as SEEP and NON-SEEP sediments, respectively. Both SEEP and NON-SEEP sediments were incubated on the anaerobic methane incubation system during two different experiments (14). During the first experiment, sediments were incubated for 27 weeks at porewater flow rates of approximately 15 to 20 cm · year^{-1} (hereafter referred to as the LF, or low-flow, experiments). The sediment cores were sampled for nucleic acid, dissolved gas, and dissolved sulfate analyses at the beginning of the incubation and at 7-, 17-, and 27-week intervals. The bottom of each sediment core was sampled at the beginning and end of the incubation to determine AOM rates. During the second experiment, sediments were incubated for 29 weeks at porewater flow rates of approximately 90 cm · year^{-1} (hereafter referred to as the HF, or high-flow, experiments), and the sediment cores were sampled as described above at 7-, 16-, and 29-week intervals.

Sample collection. During expeditions in July 2002 and February 2003 on board the research vessel *Point Lobos*, we used the remotely operated submersible *Ventana* to collect sediments from a hydrocarbon cold seep (36.75°N, 122.08°W), approximately 7 m in diameter, at a depth of 962 m in the Monterey Bay. The center of the seep consists of highly porous sediment covered by *Beggiatoa* bacterial mats, and the nearest neighboring seep is approximately 35 m away. SEEP sediment samples were collected from the center of the seep, and NON-SEEP sediments were collected from 25 m away from any visibly active seepage. All sediment samples were collected using polycarbonate-sleeve push cores (30 cm long, 5.25-cm inner diameter) that had 0.75-cm holes at 2.5-cm intervals along their length for subsampling sediments. Prior to use, these sampling ports were sealed with transparent, waterproof plastic tape to prevent leakage during sediment sample collection. Upon recovery, all push cores were sealed with butyl rubber stoppers and placed in an insulated cooler with ice packs. All sediment cores arrived in the laboratory at Moss Landing, CA, within 4 h of collection.

Sediment incubations on the AMIS. The anaerobic methane incubator system, or AMIS, is a continuous-flow bioreactor consisting of an equilibration column and gas delivery system designed to mimic sediment porewater chemistry and two manifolds that encapsulate the sediment cores (14). Filter (0.2-μm)-sterilized seawater was equilibrated with methane, hydrogen sulfide (to replicate the reducing potential found in seep sediments), and helium gas to achieve dissolved concentrations of 1.5 mM, 950 μM, and 310 μM, respectively, and was pumped through the bottom manifold as previously described (14). Filter (0.2 μm)-sterilized seawater was bubbled with air and pumped through the AMIS top manifold. A backpressure valve and hydrostatic backpressure system on both the lower and upper manifolds was used to maintain the AMIS pressures at approximately 1.01 MPa and was used to advect manifold water through the sediments (14). For the duration of all the experiments, the AMIS and seawater reservoir were maintained in a cold room at 5°C.

In a prior study, the porewater flow rate was estimated by monitoring a distinctive color change in nonseep sediments (from tan to black), an indicator of iron reduction induced by chemical reaction with hydrogen sulfide (14). In the current study, we bubbled helium into the bottom manifold seawater for use as a porewater flow tracer because it is chemically inert and cannot be metabolized.

Sediment subsampling. To subsample sediments, the AMIS manifold was enveloped in a nitrogen-purged glove bag and the sampling ports were opened. Between 2 and 2.5 g of sediment was sampled from each port using a 1-ml disposable syringe that had the tip removed with a razor blade. At least 1 g of sediment from each interval was sampled and quickly frozen in a 2-ml cryovial at −80°C for nucleic acid extraction. An additional 1 g of sediment was collected and placed into a 5-ml disposable plastic syringe containing 2 ml of a degassed 1:1 solution of ethanol and phosphate-buffered saline. The syringe was flushed with nitrogen, sealed, and shaken, and the headspace was collected in 2-ml serum vials for dissolved-gas analysis. At the beginning and end of the experiments, 5 g of sediment was collected from the 1- to 5-cm interval of each sediment core and stored in 60-ml glass syringes flushed with nitrogen and kept on ice for use in determining methane oxidation rates.

After sampling, the ports on each sediment core were sealed by compressing a 2.5-mm-thick butyl rubber sheet coated with high-vacuum grease onto the core sleeve. Plastic blocks and stainless steel hose clamps held the assembly in place.

Dissolved-gas and sulfate concentration measurements. To determine dissolved-gas concentrations, a membrane inlet mass spectrometer with a faraday cup and electron multiplier detector (Stanford Research Systems, RGA200; SRS, Inc.) was used to analyze the gas headspace of each syringe containing a sediment subsample (13, 36). Helium, methane, and hydrogen sulfide concentrations were determined by injecting 1-ml gas samples into a gastight sample chamber containing the membrane inlet, while monitoring and integrating the *m/z* peaks at 4, 15, 16, and 34, respectively, for 4 min while subtracting the background signal attributable to water. Serial dilutions of helium, methane, and hydrogen sulfide gas were used to generate standard curves (all r^2 values, >0.90). Extraction efficiency was observed to be at more than 99%. All dissolved gas concentrations are expressed as moles · gram wet weight sediment^{-1}.

Porewater dissolved sulfate concentrations were determined by turbidometric analyses (3), and absorbance was measured in a Shimadzu model 520 spectrophotometer (Shimadzu, Inc.). Serial dilutions of sodium sulfate in distilled deionized water were used to generate standard curves (all r^2 values, >0.98) to determine porewater sulfate concentrations. Sulfate concentrations are expressed as moles · gram wet weight sediment^{-1}.

Methane oxidation rate measurements. To determine methane oxidation rates, the 5-gram sediment subsamples were placed into 20-ml borosilicate glass serum vials (Kimble, Inc.). For negative controls, two seep sediment subsamples were poisoned with 2 ml of 10 M NaOH and placed into 20-ml serum vials. All vials were filled to the top with 0.2-μm-filter-sterilized anoxic seawater containing 2.0 mM methane and 1 mM hydrogen sulfide and sealed with crimp-top butyl rubber stoppers. Samples were shaken and left to incubate for 96 to 108 h. A gas-tight glass syringe, 0.2-μm-syringe filter and disposable needle were used to slowly draw a 10-ml seawater sample from the serum vial, which was analyzed by the aforementioned membrane inlet mass spectrometer. Dissolved methane partial pressures of all samples were determined by integrating the signal of both the 15 and 16 *m/z* peaks for 4 min and subtracting the background signal attributable to water (determined by examining the 16, 17, and 18 *m/z* peaks of a vacuum-degassed water sample). A standard curve was calculated by analyzing a serial dilution of methane-saturated sterile seawater standards that had been quantified using a Hewlett-Packard 5890 gas chromatograph with a molecular sieve column (Alltech, Inc.) and thermal conductivity detector. The methane concentrations before and after incubation were calculated from the standard curve (r^2 = 0.97; P = 0.0001). After incubation, half of the sediments were weighed and stored at −80°C, while the remaining sediment was weighed before and after drying at 95°C for 36 h. Specific methane oxidation rates were then calculated using the ratio of net methane oxidation rate to dry sediment mass per unit time.

Sediment nucleic acid extraction and purification. All sediment samples collected prior to and after incubation on the AMIS were weighed on an electronic balance (Mettler, Inc.), and nucleic acids were extracted as described previously (14). The nucleic acid yields were determined by fluorometric DNA quantification (PicoGreen; Molecular Probes, Inc.) using a fluorescence imaging scanner (FluorImager; ABI Biosystems, Inc.) and were correlated to the total sediment mass used in extraction. Crude nucleic acid extractions were further purified by cesium chloride buoyant-density ultracentrifugation in a Beckman TL100 benchtop ultracentrifuge (38) and were again quantified by fluorometric DNA quantification. Both the crude and cesium chloride-purified nucleic acid yields were correlated to the total sediment mass used in extraction via linear regression analyses as follows: crude nucleic acid (mg · ml^{-1}) = $-2.1e^4 + 4.9e^4$ · (sediment mass [g]); r^2 = 0.99; and purified nucleic acid (mg · ml^{-1}) = −14.255 + 0.1153 · (crude nucleic acid [mg · ml^{-1}]); r^2 = 0.99.

Design and specificity of quantitative PCR primers. To quantify ANME-1 MOA, PCR primers were designed to target the ANME-1 small-subunit rRNA gene (SSU rRNA) by using the ARB software package (24) with a database of more than 11,000 SSU rRNA sequences (ANME-1 337f = 5′-AGGTCCTACG GGACGCAT-3′; ANME-1 724r = 5′-GGTCAGACGCCTTCGCT-3′). ANME-1 primers were designed to be inclusive of the ANME-1a subgroup and do not detect the Guaymas-specific subgroup ANME-1b (35). Quantification of ANME-2c MOA was determined as previously described (14). To quantify *D*SRB, PCR primers were designed to target the SSU rRNA of *D*SRB phylotypes found in association with anaerobic methanotrophs (*D*SRB-213f = 5′–CT GTTGTTTGGAGATGAGCCC–3′; *D*SRB-658r = 5′–ATTCCACTTCCTTCT CCCATA–3′ (29). In all cases, the ARB probe design function was used to locate

TABLE 1. Nonseep sediment methane oxidation rates pre- and postincubation during low- and high-advective-flow experiments[a]

Flow regimen	Flow rate ($cm \cdot yr^{-1}$)	CH_4 oxidation rate, T_0 (nmol · g dry sediment^{-1} · day^{-1}; $N = 3$)	CH_4 oxidation rate, T_F (nmol · g dry sediment^{-1} · day^{-1}; $N = 5$)	Cell-specific methane oxidation rate, T_F (pmol CH_4 · 16 SSU copy number · day^{-1}; $N = 3$)
Low flow	≈ 19	0.30 ± 2.02	9.03 ± 1.94	0.47 ± 0.10
High flow	≈ 90	0.64 ± 3.15	138.35 ± 11.52	1.83 ± 0.17

[a] T_0, measurements prior to incubation; T_F, measurements after incubation. Values are means ± standard deviations.

group-specific sequences, and the probe match function was used to evaluate candidate primers. Primer sequences were designed with strong 3′ mismatches to closely related outgroups. Candidate primers were then screened for potentially problematic secondary structures and homo- and heterodimers using the IDT oligoanalyzer, version 3.0 (Integrated DNA Technologies, Inc.). All probes and primers were screened and optimized using Primer Express software (PE Biosystems, Inc.).

To check for possible cross-reactivity, we examined the formation of PCR products using *Beggiatoa* sp. and *Desulfobulbus sp*. genomic DNA, as well as plasmid DNA containing SSU rRNA gene fragments from 28 archaeal and bacterial phylotypes commonly found in seep sediments (29). Three-step PCRs were run in a Perkin-Elmer 9700 thermal cycler using 2.5 μl of template DNA and 22.5 μl of Platinum PCR MasterMix (Invitrogen, Inc.). The annealing temperature for all reactions was 59°C. Amplicons were then quantified against DNA standards of known concentration using the PicoGreen double-stranded DNA quantification kit (Molecular Probes, Inc.) and a fluorescent imaging scanner (FluorImager; Applied Biosystems, Inc.).

To optimize primer efficiency and specificity, a matrix of forward and reverse primer concentrations ranging from 100 to 1,500 nM was tested to determine the primer concentrations that yielded the minimal C_T values and the highest amplification efficiencies. Each primer combination was run on a Perkin-Elmer model 7700 sequence detection system (PE Biosystems, Inc.) using 2.5 μl of plasmid template and 22.5 μl of Platinum SYBR Green qPCR SuperMix UDG (Invitrogen, Inc.). All reactions were performed under the following reaction conditions: a heat soak step of 2 min at 50°C to hydrolyze residual PCR amplicons, a Platinum *Taq* activation step of 2 min at 95°C, followed by 45 cycles of 15 s at 95°C, 30 s at 59°C, and 30 s at 72°C.

Quantification of ANME-1, ANME-2c, and DSRB from sediments incubated on the AMIS. To produce a standard curve for quantification, plasmid DNA (pCR2.1) containing SSU rRNA genes from an ANME-1 phylotype (F17.1ArcA01; GenBank accession no. AY324382) and a *Desulfosarcina* sp. phylotype (Eel-24E1B12; GenBank accession no. AF354160) was quantified against a known standard using m13 forward and reverse primers (34). A serial dilution of our quantified plasmid DNA was then prepared for subsequent use as qPCR standards. CsCl-purified DNA extractions from all sediment samples were then used as template DNA in qPCR assays for ANME-1, ANME-2c, and *D*SRB. Reagent concentrations used for MOA and *D*SRB qPCR were as follows: 2.5 μl of CsCl-purified template, 1 μl ROX reference dye, 1 μl of 10 mM forward and reverse primer, and 19.5 μl of SYBR Green qPCR SuperMix UDG for a total volume of 25 μl. ANME-1 and *D*SRB qPCR reactions were run under the following conditions: a heat soak step of 2 min at 50°C to hydrolyze residual PCR amplicons, a Platinum *Taq* activation step of 2 min at 95°C, followed by 45 cycles of 15 s of 95°C, 30 s of 59°C, and 30 s of 72°C. ANME-2c assays were run as follows: a heat soak step of 2 min at 50°C to hydrolyze residual PCR amplicons and a Platinum *Taq* activation step of 2 min at 95°C, followed by 45 cycles of 15 s of 95°C, 30 s of annealing at 61°C, and 1 min of extension at 72°C.

Preliminary data suggest that ANME-1 and ANME-2 possess either two or three SSU rRNA gene copies per genome (S. Hallam, personal communication). Detection limits in all assays for ANME-1, ANME-2c, and *D*SRB ranged from 2.0×10^2, 7.5×10^1, and 3.0×10^2 SSU rRNA copies · gram sediment^{-1}, respectively.

RESULTS

Porewater flow rates and sediment chemical gradients. During the AMIS incubations, sediments were advectively irrigated with methane-saturated and sulfate-replete seawater delivered through the bottom core manifold. From the dissolved-helium measurements, we determined the porewater flow rates to be approximately 19 and 90 cm · year^{-1} during the low- and high-flow incubations, respectively (Table 1). During the low-flow incubations, bottom-manifold seawater irrigated the bottom 12 cm of the LF SEEP core and bottom 11 cm of the LF NON-SEEP core as determined by the distribution of dissolved helium in the sediments (Fig. 1C and I). During the high-flow incubations, bottom-manifold seawater irrigated the entire length of all sediment cores (Fig. 2C and I). These flow rates were corroborated by a color change from tan to black in the NON-SEEP sediment cores. In both experiments, porewater flow was about 12% faster through the SEEP sediments than NON-SEEP sediments. This is likely due to differences in sediment porosity, since the seep sediments are far more flocculent than nonseep sediments (69% and 53% porosities, respectively; data not shown).

When first collected, all SEEP sediment porewaters contained 0.4 mM or more methane throughout each core and between 16 and 28 mM sulfate from the top to the bottom of each core (note that methane concentrations cannot be accurately determined due to methane off-gassing as cores are recovered) (Fig. 1A and B; Fig. 2A and B). Both NON-SEEP sediment cores contained between 0.3 and 9 μM methane from the top to the bottom of each core and approximately 28 mM sulfate throughout the length of each core (Fig. 1G and H; Fig. 2G and H). Helium concentrations in all freshly collected sediments were below 2 nM (Fig. 1C and I; Fig. 2C and I). After both low- and high-flow incubations, SEEP and NON-SEEP sediment methane and sulfate distributions were consistent with continued advective flow of bottom manifold water, as well as depletion of methane and sulfate due to biological AOM and sulfate reduction (Fig. 1A to C and G to I; Fig. 2A to C and G to I). In the low-flow incubations, the upper 2 to 3 cm of LF SEEP and LF NON-SEEP cores showed elevated sulfate concentrations, likely due to the diffusion of seawater flowing through the top manifold (Fig. 1B and H). During the high-flow incubations, methane and sulfate concentrations in both cores varied by less than 15% of the concentrations in the bottom-manifold seawater (Fig. 2A, B, G, and H).

Distribution and population growth rates of MOA and DSRB during low- and high-flow AMIS incubations. To compare the effect of porewater flow rate on MOA and *D*SRB population growth, we estimated cell density by quantifying SSU rRNA copy number · gram sediment^{-1} via qPCR before, during, and after incubation throughout the entire sediment column. To determine the specific growth rates, we estimated cell density in the 2- to 4-cm sediment depth interval of the NON-SEEP sediment columns. This interval was chosen because it encompassed the maximum observed growth rates of both MOA and *D*SRB and was less subject to variability re-

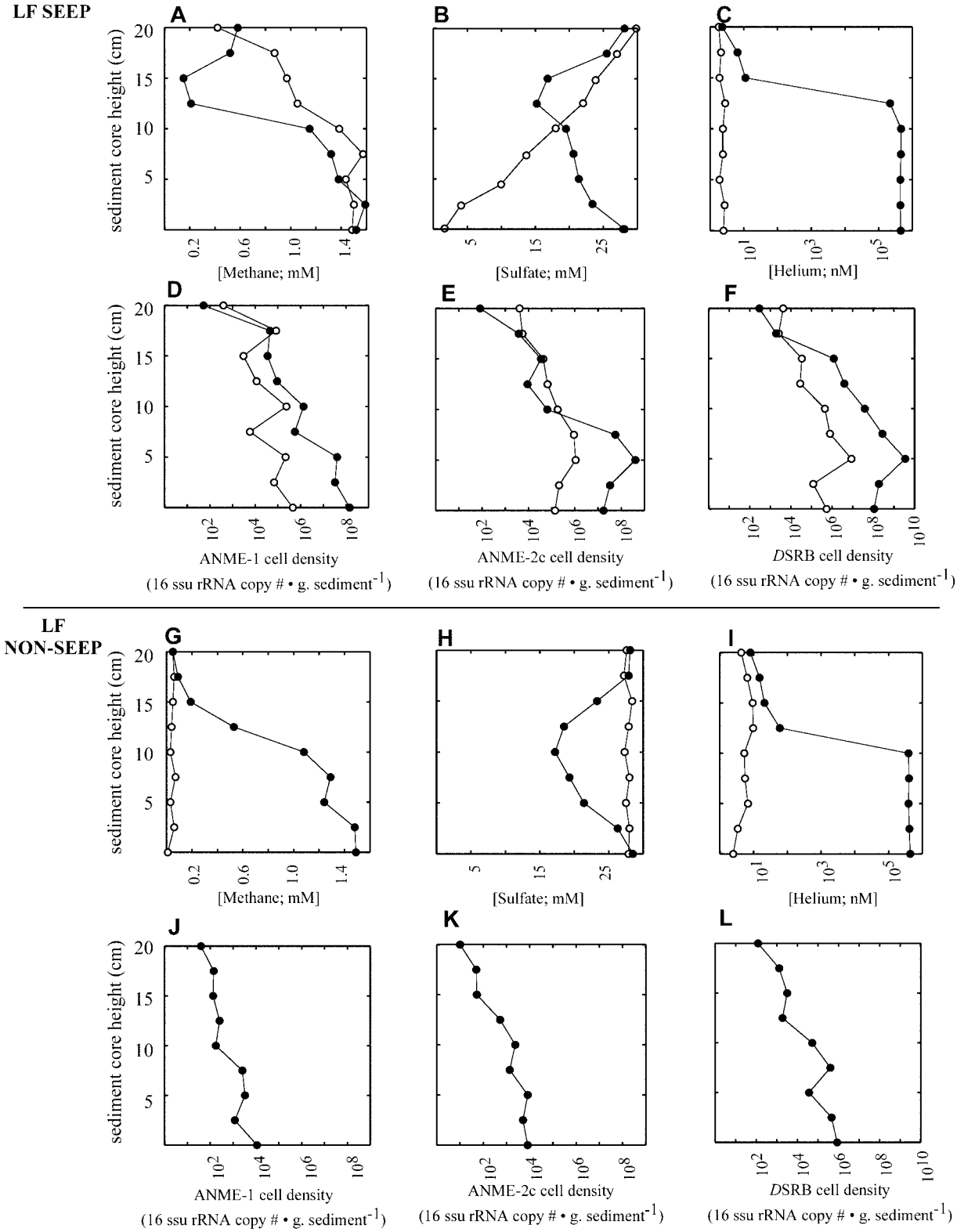

FIG. 1. Substrate concentrations (mM or nM) and cell density estimates (16 SSU rRNA gene copy number · gram sediment $^{-1}$) versus sediment core height (cm) from sediments incubated at low porewater flow rates. LF SEEP core sediments were collected from a hydrocarbon seep in Monterey bay. LF NON-SEEP sediments were collected 20 m away from visible seepage in Monterey bay. (A–C) LF SEEP methane, sulfate, and helium concentrations versus sediment core height. (D–F) LF SEEP ANME-1, ANME-2, and *D*SRB cell densities versus sediment core height. (G-I) LF NON-SEEP methane, sulfate, and helium concentrations versus sediment core height. (J–L) LF NON-SEEP ANME-1, ANME-2, and *D*SRB cell densities versus sediment core height. The absence of cell density measurements in some plots indicates that specific rRNA gene copies were below our limits of detection (typically 100 copies · g sediment^{-1}). ○ = measurements prior to incubation; ● = measurements after incubation.

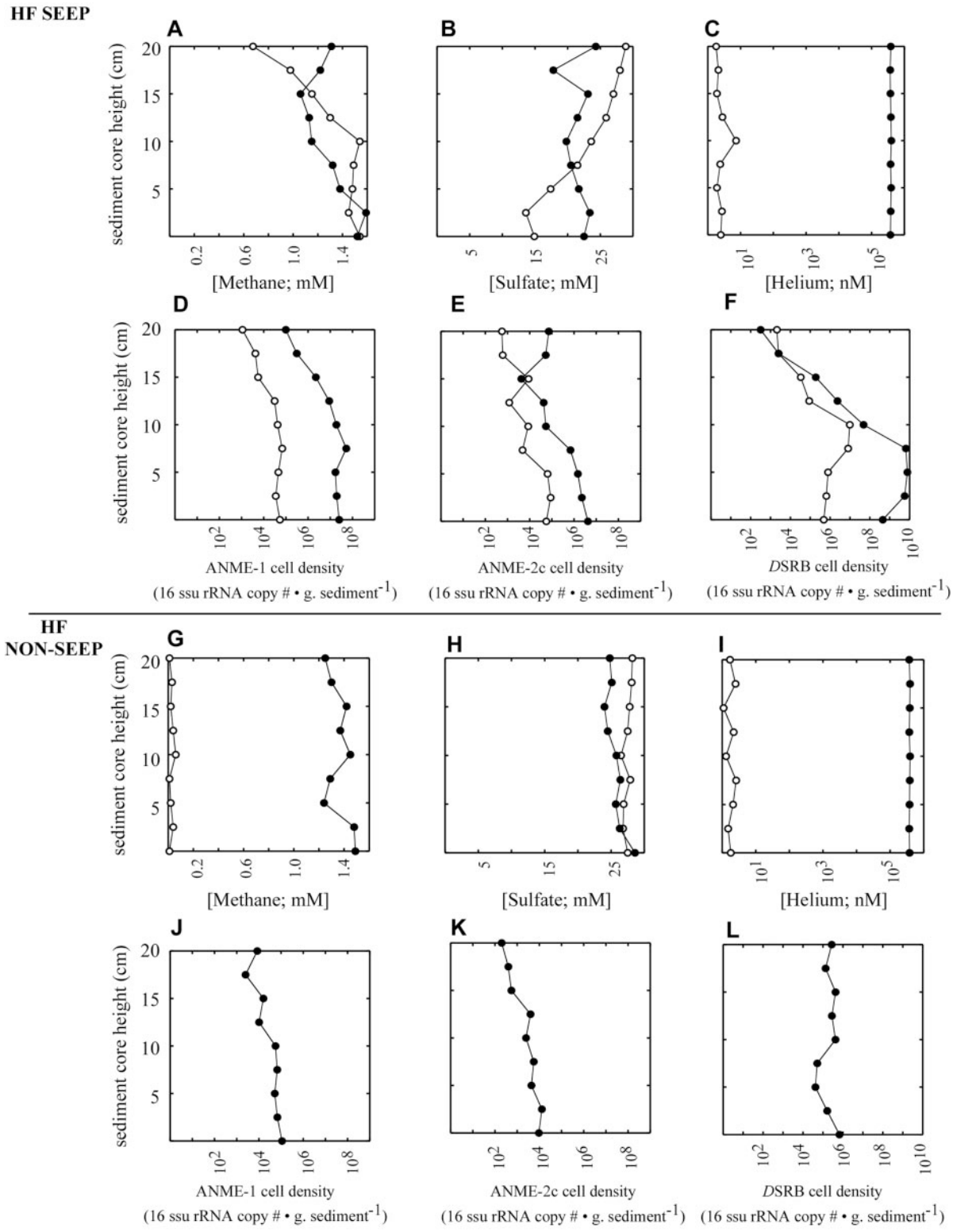

FIG. 2. Substrate concentrations (mM or nM) and cell density estimates (16 SSU rRNA gene copy number · gram sediment $^{-1}$) versus sediment core height (cm) from sediments incubated at high porewater flow rates. HF SEEP core sediments were collected from a hydrocarbon seep in Monterey bay. HF NON-SEEP sediments were collected 20 m away from visible seepage in Monterey bay. (A–C) HF SEEP methane, sulfate, and helium concentrations versus sediment core height. (D–F) HF SEEP ANME-1, ANME-2, and *D*SRB cell density versus sediment core height. (G-I) HF NON-SEEP methane, sulfate, and helium concentrations versus sediment core height. (J–L) HF NON-SEEP ANME-1, ANME-2, and *D*SRB cell density versus sediment core height. The absence of cell density measurements indicates that specific rRNA gene copies were below our limits of detection (typically 100 copies · g sediment^{-1}). ○ = measurements prior to incubation; ● = measurements after incubation.

sulting from the accumulation of debris or erosion of sediment that can occur at the sediment-bottom water interface. Calculating the specific growth rates from the NON-SEEP sediments also reduced the possibility that MOA and *D*SRB growth would be influenced by preexisting factors found in seep sediments, such as differences in MOA or *D*SRB populations before incubation. Prior studies of anoxic marine sediments have observed large differences of MOA population density over small spatial scales that reflect the physicochemical variations found in situ (14, 31).

Prior to the low-flow incubations, ANME-1, ANME-2, and *D*SRB cell density estimates within the SEEP sediments were between 6.7×10^2 and 1.4×10^7 SSU rRNA copies · gram sediment^{-1} (Fig. 1D to F), while the ANME-1, ANME-2, and *D*SRB cell densities in the NON-SEEP sediment were below our limits of detection. At the end of the low-flow incubation, ANME-1 and ANME-2c cell density estimates had typically increased between two and four orders of magnitude in the bottom 5 cm of sediment of both the SEEP and NON-SEEP sediments (the approximate extent of bottom-manifold water advection) (Fig. 1D to F and J to L). ANME-1 and ANME-2c cell density estimates in the upper 4 cm of the SEEP core remained comparable or decreased between one and two orders of magnitude, respectively, by the end of the incubation (Fig. 1D to F). In both SEEP and NON-SEEP incubations, *D*SRB cell density estimates typically showed increases between one and four orders of magnitude and were most prevalent in the lower 10 cm of both SEEP and NON-SEEP sediment cores (Fig. 1F and L).

During the low-flow incubations, maximum specific growth rates (μ) of ANME-1 MOA, ANME-2c MOA, and *D*SRB in the 2- to 4-cm interval of the LF NON-SEEP core were 0.121, 0.167, and 0.302 · week^{-1}, respectively (*G* [generation time] = 40, 29, and 16 days, respectively) (Fig. 3A). The cell density estimates of ANME-1 MOA, ANME-2c MOA and *D*SRB reached 4.5×10^3 and 8.9×10^3 and 6.7×10^5 SSU rRNA copies · gram sediment^{-1}, respectively (Fig. 3A).

Prior to the high-flow incubations, ANME-1, ANME-2, and *D*SRB MOA cell density estimates within the SEEP sediments ranged between 8.2×10^2 and 1.1×10^7 SSU rRNA copies · gram sediment^{-1} (Fig. 2D to F), while the ANME-1, ANME-2c, and *D*SRB cell densities in the NON-SEEP sediments were below our limits of detection. At the end of the high-flow incubation, ANME-1 cell density estimates in the HF SEEP core, as well as the HF NON-SEEP core, had typically increased between two and four orders of magnitude throughout the SEEP and NON-SEEP sediments (Fig. 2D and J). ANME-2c cell density estimates, however, typically increased between one and two orders of magnitude throughout the SEEP and NON-SEEP sediments (Fig. 2E and K). *D*SRB cell density changes in the SEEP sediments were highly variable, ranging from population decreases to increases greater than four orders of magnitude (Fig. 2F and L). *D*SRB cell densities showed the largest increases in the NON-SEEP sediments, between three and five orders of magnitude (Fig. 2L).

During the high-flow incubations, the specific growth rates (μ) of ANME-1 and ANME-2c MOA and *D*SRB in the HF NON-SEEP core were 0.218, 0.158, and 0.286 · week^{-1}, respectively (G = 22, 31, and 17 days, respectively) (Fig. 3B). The cell density estimates of ANME-1 MOA, ANME-2 MOA, and *D*SRB in the 2- to 3-cm interval of the LF NON-SEEP core reached 1.2×10^5, 9.1×10^3, and 1.2×10^7 SSU rRNA copies · gram sediment^{-1}, respectively (Fig. 3B).

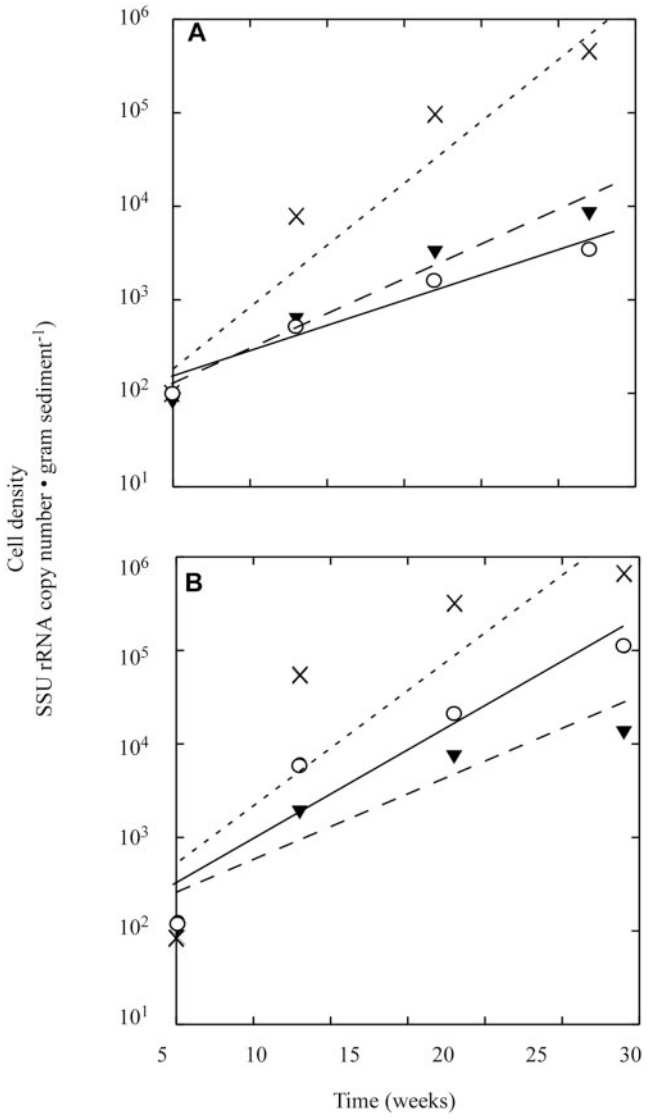

FIG. 3. (A) ln(cell density) versus time from a nonseep sediment core incubated with low porewater flow rates. Linear regressions representing the best fit between the ln(cell density) and time in the low-flow incubations are as follows: ln(ANME-1) = $160.4 \cdot e^{0.121x}$; r^2 = 0.98; ln(ANME-2) = $124.9 \cdot e^{0.167x}$; r^2 = 0.98; ln(*D*SRB) = $274.2 \cdot e^{0.302x}$; r^2 = 0.98. (B) ln(cell density) versus time from a nonseep sediment core incubated with higher porewater flow rates. Linear regressions representing the best fit between ln(cell density) and time in the higher-flow incubations are as follows: ln(ANME-1) = $321.3 \cdot e^{0.218x}$; r^2 = 0.99; ln(ANME-2) = $230.4 \cdot e^{0.158x}$; r^2 = 0.93; ln(*D*SRB) = $613.4 \cdot e^{0.286x}$; r^2 = 0.91. ANME-1 = ○; ANME-2 = ▼; *D*SRB = ×.

Methane oxidation rates during low and high flow AMIS incubations. Prior to incubations, we were unable to detect AOM in either the LF NON-SEEP or HF NON-SEEP sediments (Table 1). After the low flow incubation, the AOM rate measured in the bottom 2 cm of the LF NON-SEEP sediment was 9.03 ± 1.94 nmol · gram dry sediment^{-1} · day^{-1} (Table 1). After the high flow incubation, the AOM rate measured in the

bottom 2 cm of the HF NON-SEEP sediment was 138.35 ± 11.52 nmol CH_4 · g dry sediment^{-1} · day^{-1}, a significantly higher rate than in the low flow experiment ($P = 0.0001$; Mann Whitney U-test). When AOM rates were expressed with respect to MOA cell density estimates, sediments from low and high porewater flow experiments exhibited rates of 0.57 ± 0.10 and 1.83 ± 0.17 pmol CH_4 · SSU rRNA copy number · day^{-1}, respectively, and were significantly different ($P > 0.0001$, Mann Whitney U-test; Table 1). AOM rates of the SEEP sediments in both the low and high flow incubations ranged from 29.11 to 154.52 nmol · gram dry sediment^{-1} · day^{-1}, and were not statistically significantly different before and after incubation.

DISCUSSION

In light of the relatively low energy yields expected from the anaerobic oxidation of methane, estimates of MOA growth rates have been the subject of much speculation (18, 20, 26). Our data show that MOA populations, when stimulated by contact with the advected methane and sulfate-laden porewater, are metabolically active and are capable of substantial growth rates at low temperatures (Table 1; Fig. 3). We also observed that MOA generation times increase to 95 days in sediments that were not exposed to advected porewater (e.g., in the upper 4 cm of the LF SEEP core [Fig. 1]). However, none of the rates presented here should be construed as maximal growth rates, since it is possible that higher-pressure incubations (with higher dissolved-methane concentrations) or other variations in environmental conditions would result in more rapid MOA growth rates. Future AMIS incubations at in situ pressure and with variable methane concentrations and temperature will explore these issues.

The most rapid MOA specific growth rates presented here are comparable to some known psychrophilic methanogens (10). The specific growth rates of three methylotrophic methanogens isolated from permanently cold (<6°C) marine sediments in Skan Bay, Alaska, are predicted to range from 0.133 to 0.322 · week^{-1} (D. Boone, personal communication). Conversely, *Methanosarcina lacustris*, a psychrotolerant member of methylotrophic archaea, has a specific growth rate of 0.504 · week^{-1} at 5°C (33), while *Methanogenium frigidum* sp. nov., a hydrogenotrophic methanogen, has a specific growth rate of 0.7 · week^{-1} at 5°C (11). The latter specific growth rates are 4 to 6 time higher than that of MOA and may be attributable to the higher energy yields from hydrogenotrophic or methylotrophic methanogenesis (10). However, other factors, such as growth yield and substrate-specific consumption rates, have yet to be determined for both MOA and these archaea and may provide further insight into these differences.

The flow rate experiments presented here provide the first tractable, albeit circumstantial, insights into MOA population dynamics. These data suggest that the porewater flow rate, or some covarying factor, differentially influences ANME-1 and ANME-2 MOA population growth dynamics. ANME-1 generation time increased by 45% during the higher-flow experiment, whereas ANME-2 doubling times were minimally affected by increased flow rate (Fig. 3). By the end of the high-flow experiments, ANME-1 cell density had exceeded the ANME-2 cell density significantly (for comparison, the ANME-2 population exceeded the ANME-1 population by just fourfold at the end of the low-flow experiments) (Fig. 3). In both cases, the initial cell densities of ANME-1 and ANME-2 were undetectable, so it is unlikely that these results are due to a "founder effect" (in which one phylotype dominates an ecosystem via its numerical advantage). These data suggest that in higher-flow regimes, ANME-1 MOA may be able to outgrow and outcompete ANME-2 MOA for resources. This may serve to explain field observations of MOA distributions, where the ANME-1 group seems to exist in higher flow regimes than ANME-2 (26, 31). Although in vitro experiments with MOA found that changing key environmental parameters, such as sulfate concentration, pH, and salinity, did not differentially influence the activity of ANME-1 and ANME-2 communities (28), future experiments should attempt to discern if these or other covarying factors (such as micronutrient availability or end product elimination) differentially influence ANME-1 and ANME-2 population growth rates.

*D*SRB population growth rates were similar in both low- and high-flow incubations (Fig. 3) and were comparable to those of other psychrophilic sulfate-reducing bacteria isolated from cold sediments (21). Although *D*SRB growth rates during both incubations were substantially more rapid than the MOA growth rates in the same sediment interval, *D*SRB population growth was not constant over time during the high-flow incubations (Fig. 3B). *D*SRB population growth appeared diauxic, with a putatively higher specific growth rate during the first 7 weeks of incubation ($\mu_{DSRB} = 0.815 \cdot \text{week}^{-1}$, $G_{DSRB} = 5.9$ days; regression not shown). The *D*SRB growth rate appeared to decrease after the first 7 weeks of incubation ($\mu_{DSRB} = 0.120 \cdot \text{week}^{-1}$; $G_{DSRB} = 41$ days; regression not shown). We suggest that *D*SRB population growth may not initially depend on an established MOA population and instead may rely on metabolizing endogenous organics. Data from preliminary experiments in which we used the AMIS bioreactor to deliver anoxic seawater containing 200 μM sodium acetate to nonseep sediments show that rapid *D*SRB growth rates at 5°C can be achieved in the absence of detectable MOA growth ($\mu_{DSRB} = 0.416 \cdot \text{week}^{-1}$; data not shown). In nature, sulfate-reducing bacteria are capable of growth on a variety of reduced organics and flourish in diverse environments, including those devoid of AOM (12, 17). After a substantial and active MOA population is established, *D*SRB growth may be more governed by syntrophy with MOA.

While we were able to measure *D*SRB population growth, our *D*SRB primers were designed to target phylotypes previously observed to form associations with MOA (5, 29). These primers do not target all sulfate-reducing bacteria (6), and it is likely that some fraction of the *D*SRB population was not detected in this study. Future experiments should examine a wider variety of sulfate-reducing phylotypes to better assess the relation between MOA and other groups of sulfate-reducing bacteria.

The total methane oxidized also increased as a function of the larger MOA biomass, as did the cell-specific methane oxidation rate per unit cell (which increased 3.8-fold between the lower and higher porewater flow regime experiments) (Table 1). Because all conditions (except for flow rate) in both incubations were comparable, we surmise that the increased cell-specific methane oxidation rate in the high-flow experiments

may be attributable to increases in metabolic cost associated with cell division. This supposition, however, should be further addressed.

Studying the physiology of microbes in situ is fraught with difficulties due to the inherent complexity of natural systems. Likewise, overly simplistic laboratory studies in static systems may not well represent the physicochemical dynamics found in nature. Laboratory-based bioreactors, such as AMIS, better approximate in situ conditions, are not likely to lead to substrate depletion or end product inhibition that can occur in static incubations (1, 8, 9, 16, 20, 27, 40), and consequently can provide insights into microbial community dynamics, such as population growth, inter- and intraphylotypic competition, and biogeochemical linkages. The results presented here demonstrate that MOA and *D*SRBs can attain substantial populations over the range of environmental conditions used in these experiments, despite the relatively low methane concentrations available at lower pressures.

ACKNOWLEDGMENTS

We thank Christina Preston, Lynne Christianson, and Steven Hallam for their many relevant discussions, Marcelino Suzuki for his continued tutelage, and the crew of the research vessel *Point Lobos* and the pilots of the remotely operated vehicle *Ventana* for their tireless support and efforts.

This work was supported by a grant from the Gordon and Betty Moore Foundation, NSF grant MCB 0024811, and the Packard Foundation, all to E.F.D.

REFERENCES

1. **Alperin, M. J., and W. S. Reeburgh.** 1985. Inhibition experiments on anaerobic methane oxidation. Appl. Environ. Microbiol. **50:**940–955.
2. **Amann, R. I., W. Ludwig, and K. H. Schleifer.** 1995. Phylogenetic identification and *in situ* detection of individual microbial cells without cultivation. Microbiol. Rev. **59:**143–169.
3. **American Public Health Association.** 1992. Standard methods for the examination of water and wastewater, 18th ed., p. 4–134. American Public Health Association, Washington, D.C.
4. **Barnes, R. O., and E. D. Goldberg.** 1976. Methane production and consumption in anoxic marine sediments. Geology **4:**297–300.
5. **Boetius, A., K. Ravenschlag, C. J. Schubert, D. Rickert, F. Widdel, A. Gieseke, R. Amann, B. B. Jorgensen, U. Witte, and O. Pfannkuche.** 2000. Microscopic identification of a microbial consortium apparently mediating anaerobic methane oxidation above a marine gas hydrate. Nature **407:**623–626.
6. **Daly, K., R. J. Sharp, and A. J. McCarthy.** 2000. Development of oligonucleotide probes and PCR primers for detecting phylogenetic subgroups of sulfate-reducing bacteria. Microbiology **146:**1693–1705.
7. **DeLong, E. F., G. Wickham, and N. R. Pace.** 1989. Phylogenetic stains: ribosomal RNA-based probes for identification of single microbial cells. Science **243:**1360–1363.
8. **Devol, A. H.** 1983. Methane oxidation rates in the anaerobic sediments of Saanich Inlet. Limnol. Oceanogr. **28:**738–742.
9. **Devol, A. H., and S. L. Ahmed.** 1981. Are high rates of sulfate reduction associated with anaerobic methane oxidation? Nature **291:**407–408.
10. **Ferry, J. G.** 1993. Methanogenesis: ecology, physiology, biochemistry & genetics. Chapman & Hall, New York, N.Y.
11. **Franzmann, P., Y. Liu, D. Balkwill, H. Aldrich, E. E. Conway de Macario, and D. Boone.** 1997. *Methanogenium frigidum* sp. nov., a psychrophilic, H_2-using methanogen from Ace Lake, Antarctica. Int. J. Syst. Bacteriol. **47:**1068–1072.
12. **Gibson, G.** 1990. Physiology and ecology of the sulphate-reducing bacteria. J. Appl. Bacteriol. **69:**769–797.
13. **Girguis, P. R., R. W. Lee, N. Desaulniers, J. J. Childress, M. Pospesel, H. Felbeck, and F. Zal.** 2000. Fate of nitrate acquired by the tubeworm *Riftia pachyptila*. Appl. Environ. Microbiol. **66:**2783–2790.
14. **Girguis, P. R., V. J. Orphan, S. J. Hallam, and E. F. DeLong.** 2003. Growth and methane oxidation rates of anaerobic methanotrophic archaea in a continuous-flow bioreactor. Appl. Environ. Microbiol. **69:**5472–5482.
15. **Hallam, S. J., N. Putnam, C. M. Preston, J. C. Detter, D. Rokhsar, P. Richardson, and E. F. DeLong.** 2004. Reverse methanogenesis: testing the hypothesis with environmenal genomics. Science **305:**1457–1462.
16. **Hansen, L. B., K. Finster, H. Fossing, and N. Iversen.** 1998. Anaerobic methane oxidation in sulfate-depleted sediments: effects of sulfate and molybdate additions. Aquat. Microb. Ecol. **14:**195–204.
17. **Hansen, T. A.** 1994. Metabolism of sulfate-reducing prokaryotes. Antonie Leeuwenhoek **66:**165–185.
18. **Harder, J.** 1997. Anaerobic methane oxidation by bacteria employing (super 14) C-methane uncontaminated with (super 14) C-carbon monoxide, p. 13–23. *In* T. C. E. van Weering, G. T. Klaver, and R. A. Prins (ed.), Marine geology, vol. 137. Elsevier, Amsterdam, The Netherlands.
19. **Hinrichs, K.-U., J. M. Hayes, S. P. Sylva, P. G. Brewer, and E. F. DeLong.** 1999. Methane consuming archaebacteria in marine sediments. Nature **398:**802–805.
20. **Hoehler, T. M., M. J. Alperin, D. B. Albert, and C. S. Martens.** 1994. Field and laboratory studies of methane oxidation in an anoxic marine sediment: Evidence for a methane-sulfate reducer consortium. Global Biogeochem. Cycles **8:**451–463.
21. **Knoblauch, C., and B. B. Jorgensen.** 1999. Effect of temperature on sulphate reduction, growth rate and growth yield in five psychrophilic sulphate-reducing bacteria from Artic sediments. Environ. Microbiol. **1:**457–467.
22. **Kotelnikova, S.** 2002. Microbial production and oxidation of methane in deep subsurface. Earth-Science Rev. **58:**367–395.
23. **Kruger, M., A. Meyerdierks, F. O. Glockner, R. Amann, F. Widdel, M. Kube, R. Reinhardt, J. Kahnt, R. Bocher, R. Thauer, and S. Shima.** 2003. A conspicuous nickel protein in microbial mats that oxidize methane anaerobically. Nature **426:**878–881.
24. **Ludwig, W., O. Strunk, R. Westram, L. Richter, H. Meier, A. Buchner, T. Lai, S. Steppi, G. Jobb, W. Förster, I. Brettske, S. Gerber, A. W. Ginhart, O. Gross, S. Grumann, S. Hermann, R. Jost, A. König, T. Liss, R. Lüβmann, M. May, B. Nonhoff, B. Reichel, R. Strehlow, A. P. Stamatakis, N. Stuckmann, A. Vilbig, M. Lenke, T. Ludwig, A. Bode, and K.-H. Schleifer.** 2004. ARB: a software environment for sequence data. Nucleic Acids Res. **32:**1363–1371.
25. **Martens, C. S., and R. A. Berner.** 1974. Methane production in the interstitial waters of sulfate-depleted marine sediments. Science **185:**1167–1169.
26. **Michaelis, W., R. Seifert, K. Nauhaus, T. Treude, V. Thiel, M. Blumenberg, K. Knittel, A. Gieske, K. Peterknecht, T. Pape, A. Boetius, R. Amann, B. B. Jorgensen, F. Widdel, J. Peckmann, N. Pimenov, and M. Gulin.** 2002. Microbial reefs in the Black Sea fueled by anaerobic oxidation of methane. Science **297:**1013–1015.
27. **Nauhaus, K., A. Boetius, M. Kruger, and F. Widdel.** 2002. In vitro demonstration of anaerobic oxidation of methane coupled to sulfate reduction in sediment from a marine gas hydrate area. Environ. Microbiol. **4:**296–305.
28. **Nauhaus, K., T. Treude, A. Boetius, and M. Kruger.** 2005. Environmental reulgation of the anaerobic oxidation of methane: a comparison of ANME-1 and ANME-2 communities. Environ. Microbiol. **7:**98–106.
29. **Orphan, V. J., K.-U. Hinrichs, W. Ussler III, C. K. Paull, L. T. Taylor, S. P. Sylva, J. M. Hayes, and E. F. DeLong.** 2001. Comparative analysis of methane-oxidizing archaea and sulfate-reducing bacteria in anoxic marine sediments. Appl. Environ. Microbiol. **67:**1922–1934.
30. **Orphan, V. J., C. H. House, K.-U. Hinrichs, K. D. McKeegan, and E. F. DeLong.** 2002. Multiple archaeal groups mediate methane oxidation in anoxic cold seep sediments. Proc. Natl. Acad. Sci. USA **99:**7663–7668.
31. **Orphan, V. J., W. Ussler III, T. H. Naehr, C. H. House, K. U. Hinrichs, and C. K. Paull.** 2004. Geological, geochemical, and microbiological heterogeneity of the seafloor around methane vents in the Eel River Basin, offshore California. Chem. Geol. **205:**265–289.
32. **Reeburgh, W. S.** 1976. Methane consumption in Cariaco Trench waters and sediments. Earth Planetary Sci. Lett. **28:**337–344.
33. **Simankova, M., S. Parshina, T. Tourova, T. Kolganova, A. Zehnder, and A. Nozhevnikova.** 2001. *Methanosarcina lacustris* sp. nov., a new psychrotolerant methanogenic archaeon from anoxic lake sediments. Syst. Appl. Microbiol. **24:**362–367.
34. **Suzuki, M. T., L. T. Taylor, and E. F. DeLong.** 2000. Quantitative analysis of small subunit ribosomal RNA genes in mixed microbial populations employing 5′-nuclease assays. Appl. Environ. Microbiol. **66:**4605–4614.
35. **Teske, A., K.-U. Hinrichs, V. Edgcomb, A. de Vera Gomez, D. Kysela, S. P. Sylva, L. S. Mitchell, and H. W. Jannasch.** 2002. Microbial diversity of hydrothermal sediments in the Guaymas Basin: evidence for anaerobic methanotrophic communities. Appl. Environ. Microbiol. **68:**1994–2007.
36. **Thomas, K. L., D. Lloyd, J. Benstead, and S. H. Lloyd.** 1998. Diurnal oscillations of gas production and effluxes ($C0_2$ and CH_4) in cores from a peat bog. Biol. Rhythm Res. **29:**247–259.
37. **Tsunogai, U., N. Yoshida, and T. Gamo.** 2002. Carbon isotopic evidence of methane oxidation through sulfate reduction in sediment beneath cold seep vents on the seafloor at Nankai Trough, p. 145–160. *In* P. Huchon and H. Tokuyama (ed.), Marine geology, vol. 187. Elsevier, Amsterdam, The Netherlands.
38. **Weeks, D. P., N. Beerman, and O. M. Griffith.** 1986. A small-scale five-hour procedure for isolating multiple samples of CsCl-purified DNA: application

to isolations from mammalian, insect, higher plant, algal, yeast, and bacterial sources. Anal. Biochem. **152:**376–385.

39. **Werne, J. P., J. S. Sinninghe Damste, et al.** 2001. Molecular isotopic evidence for carbon-cycling in anaerobic methane oxidizing microbial communities in eastern Mediterranean mud volcanos, p. 224. Abstracts with Programs: Geological Society of America, vol. 33. Geological Society of America, Boulder, Colo.
40. **Zehnder, A. J., and T. D. Brock.** 1980. Anaerobic methane oxidation: occurrence and ecology. Appl. Environ. Microbiol. **39:**194–204.
41. **Zhang, C. L., Y. Li, J. D. Wall, L. Larsen, R. Sassen, Y. Huang, Y. Wang, A. Peacock, D. C. White, J. Horita, and D. R. Cole.** 2002. Lipid and carbon isotopic evidence of methane-oxidizing and sulfate-reducing bacteria in association with gas hydrates from the Gulf of Mexico. Geology **30:**239–242.